Contents lists available at ScienceDirect

Transactions of Nonferrous Metals Society of China

36(2026) 709−726

www.tnmsc.cn

Strengthening mechanism of 2195 Al−Li alloy by thermomechanical treatment based on impact hydroforming loading

Hong-liang ZHU [a,b], Yong XU [a,b,*], Wen-long XIE [a,b], Shi-hong ZHANG [a,b], Xiu-wen LV [a,b], Muhammad Farooq SALEEM [a,b], Artur I. POKROVSKY [c], Boris B. KHINA[c]

[a] Institute of Metal Research, Chinese Academy of Sciences, Shenyang 110016, China;
[b] School of Materials Science and Engineering, University of Science and Technology of China, Shenyang 110016, China;
[c] Physical-Technical Institute, National Academy of Science of Belarus, Minsk 2200084, Belarus

Abstract: A novel method called thermomechanical treatment based on impact hydroforming (TTIHF) was proposed. The pre-deformation was achieved by using impact hydroforming (IHF) loading. The strengthening effect and mechanism of 2195 Al−Li alloy were investigated under various loading pre-deformation conditions. The results showed that the time for the alloy to reach peak aging was shortened under TTIHF. Compared with those of the pre-deformation method of stamping forming, the yield strength and tensile strength of the Al−Li alloy under TTIHF increased by 18.6% and 18.0%, respectively. The deformation caused by IHF loading resulted in a high density of dislocations, which served as nucleation sites for the precipitation of the T_1 phase during aging. After TTIHF, the average diameter and thickness of the T_1 phase in the alloy were smaller than those under other experiment conditions. Moreover, the density and distribution of the T_1 phase were the highest and the most uniform.

Keywords: Al−Li alloy; thermomechanical treatment; impact hydroforming; peak aging; strengthening mechanism; dislocation density

1 Introduction

The addition of lithium to an aluminum alloy results in the formation of aluminum lithium (Al−Li) alloys. The presence of 1 wt.% Li reduces the density of the material by approximately 3% while simultaneously raising the elastic modulus by 5%−6% [1,2]. Al−Li alloys possess numerous unique advantages [3] such as reduced structural weight and increased stiffness [4,5] in comparison to conventional high-strength aluminum alloys. Therefore, Al−Li alloys are considered ideal for application in the aerospace industry as a structural material with extensive potentiality [6−9]. Currently, Al−Li alloys are being used in aerospace and launch vehicles, military and passenger aircrafts. They are mostly employed in the fuselage skin, floor beams, and fuselage frame [10]. However, besides the issues of poor formability and easy cracking at room temperature, the investigation into the heat treatment of Al−Li alloys still remains incomplete. Thus, the problem of improving comprehensive properties of Al−Li alloys through an appropriate heat treatment process is one of the main focuses of many researchers.

The strength of an Al−Li alloy can be significantly enhanced through the process of solution and aging treatment since it is a type of alloy that can be reinforced by heat treatment [11]. The pre-deformation before aging generates a large number of dislocations [12], thus providing nucleation sites for subsequent T_1 precipitates and substantially improving the nucleation rate of T_1

Corresponding author: *Yong XU, Tel: +86-24-23906831, E-mail: yxu@imr.ac.cn
https://doi.org/10.1016/S1003-6326(25)66992-5
Received 9 July 2024; accepted 28 February 2025

phase, which will significantly enhance the strength of the alloy [13]. Thermomechanical treatment (TMT) is a composite method that combines the strengthening effects of plastic deformation and heat treatment phase transition. CASSADA et al [14], and NOBLE and THOMPSON [15] discovered that pre-deformation before aging can alter the competitive precipitation kinetics of the T_1 (Al_2CuLi) phase and δ' (Al_3Li) phase and promote the precipitation of the T_1 phase. At the same time, the generation of dislocations in the alloy during the pre-deformation before aging will prevent the precipitation of δ' phase and make it easier for the T_1 phase to precipitate. XIE et al [16] investigated the effects of aging temperature, single/double stage aging regime, and amount of pre-deformation on the precipitation behavior of 2195 Al−Li alloys. The results indicate that dislocations generated by pre-deformation can directly enhance strain hardening, while indirectly improving precipitation strengthening by refining the size of the T_1 phase particles and increasing their number. It has also been found that the mechanical properties and fracture modes of materials are related to dislocation density, as well as to the type, size, distribution, and quantity of precipitates. CHEN et al [17] found that the dislocations introduced by pre-deformation can promote more uniform precipitation of finely dispersed precipitates and reduce the anisotropy of the alloy. An increase in the number density of the T_1 phase precipitates and the improvement of their distribution uniformity are the main reasons for reducing the anisotropy of mechanical properties. The elimination of precipitate-free zone (PFZ) and an increase in grain boundary strength also contribute to the reduction of anisotropy. LI et al [18] investigated the effect of rolling pre-deformation on the formation of T_1 phase and $\delta'/\theta'/\delta$ composite precipitates in Al−Cu−Li−Mg alloys. The results have shown that 5% pre-deformation can promote the formation of the T_1 phase, inhibit the formation of $\delta'/\theta'/\delta$ composite precipitates, and improve the strength of the alloy, but significantly reduce its plasticity. LI et al [19] compared the effect of TMT on the 2219 aluminum alloy under three different pre-deformation conditions: tension, compression, and rolling. When the tensile strain at pre-deformation is 8.0%, the yield strength reaches 385.0 MPa, which is 22.2% higher than that without pre-deformation. When the thinning ratio at compression deformation is 4.0%, the maximum tensile strength of the alloy attains 472.4 MPa, indicating that the strengthening effect of thermomechanical treatment is higher than that of ordinary heat treatment.

The pre-deformation methods mentioned above were all low strain rate deformations. Recently, some researchers have begun to explore the high strain rate (HSR) forming combined with heat treatment methods to develop a novel TMT process in order to enhance comprehensive properties of materials. XU et al [20] proposed an electromagnetic deformation combined with heat treatment, which consists of solution quenching, electromagnetic deformation and artificial aging, and can be applied to forming high-performance Al−Li alloy components. The results have shown that compared with the traditional TMT process, electromagnetic deformation as a HSR loading can efficiently improve the strength of the alloy after heat treatment [20,21]. XIE et al [22] proposed a hot electromagnetic forming process, and compared with quasistatic tension, the morphology and density of dislocations formed by electromotive force appeared to be different, which further increased the number of nucleation sites of the T_1 phase and improved the aging kinetics.

Impact hydroforming (IHF) is a novel HSR forming process, which combines the advantages of the flexibility of hydroforming and specific features of HSR deformation [23]. The IHF technique utilizes the energy from a high-speed impact projectile to generate an impulse of a high hydraulic pressure in a liquid medium. This replaces the static high-pressure output typically achieved by a booster in traditional hydroforming. Following one or more impacts, the blank rapidly conforms to the die, which results in the formation of a final part [23]. The IHF technology has the advantages of a high-impact energy, short forming time, adjustable initial energy, and can be used for a wide range of applications. In recent years, it has been demonstrated that IHF, as the novel plastic processing technology, can greatly enhance the formability of low-plasticity materials, including lightweight alloys such as aluminum and titanium alloys [24,25]. AZARYAN et al [26] designed an IHF equipment based on compressed gas as the power source and performed process development for some typical parts made of different materials including steel, aluminum, and titanium alloys. AKST et al [27] and HOMBERG et al [28] also developed IHF equipment using compressed gas

as the power source. In addition, they studied the factors affecting the movement of the impact projectile, and explored the relationship between the measured and theoretically calculated kinetic energy of the experimental projectile. The research by XIA et al [29] has shown that the IHF technology can achieve the integration of shape and performance control of parts, thereby establishing the basis for further advancement of high-strength lightweight alloys commonly used in the aerospace industry. ZHANG et al [24] and LI et al [30] investigated the deformation behavior of various aluminum alloys and the Ti−6Al−4V alloy at a room temperature, using a wide range of strain rates. It has been found that under high strain rates (>10^3 s^{-1}) the formability is significantly improved and spring-back is efficiently reduced. An analytical model was established to predict the spring-back behavior of Ti−6Al−4V alloy at a room temperature, considering the effects of deformation history and strain rate.

However, currently, there is a lack of research reports on the combination of IHF and heat treatment technology. So, in this study, a novel TMT process technology called the thermomechanical treatment based on impact hydroforming (TTIHF) was proposed, which included solution treatment, deformation by IHF loading, and artificial aging. Simultaneously, two control experiments were conducted, namely heat treatment without deformation (HTWD) and thermomechanical treatment based on rigid punch stamping forming (TTSF). The mechanical properties, microstructure evolution and precipitation aging behavior of 2195 Al−Li alloy under various conditions were also investigated. The strengthening mechanism of Al−Li alloy after TTIHF was revealed, which provided a new concept for the HSR thermomechanical treatment of a third-generation Al−Li alloy.

2 Experimental

2.1 Materials and testing methods

A 2195-O Al−Li alloy sheet was used as the material that can be strengthened by means of heat treatment. The thickness of the sheet was 1.3 mm. Figures 1(a) and (b) show the initial microstructure and statistical distribution of the grain size of the 2195 Al−Li alloy, respectively. Based on statistical data, the mean grain size is 52.58 μm. A room-temperature tensile test was performed using a WDW−100KN electronic universal testing machine with a tensile speed of 1.44 mm/min. All tensile specimens were cut from the sheet along the rolling direction (RD); the size and cutting method are shown in Figs. 1(c) and (d), respectively. To ensure the accuracy and repeatability of the results, two samples were used as a control group in each experiment. The phase analysis of the 2195 Al−Li alloy was carried out by X-ray diffraction (XRD) to observe the position and intensity of diffraction

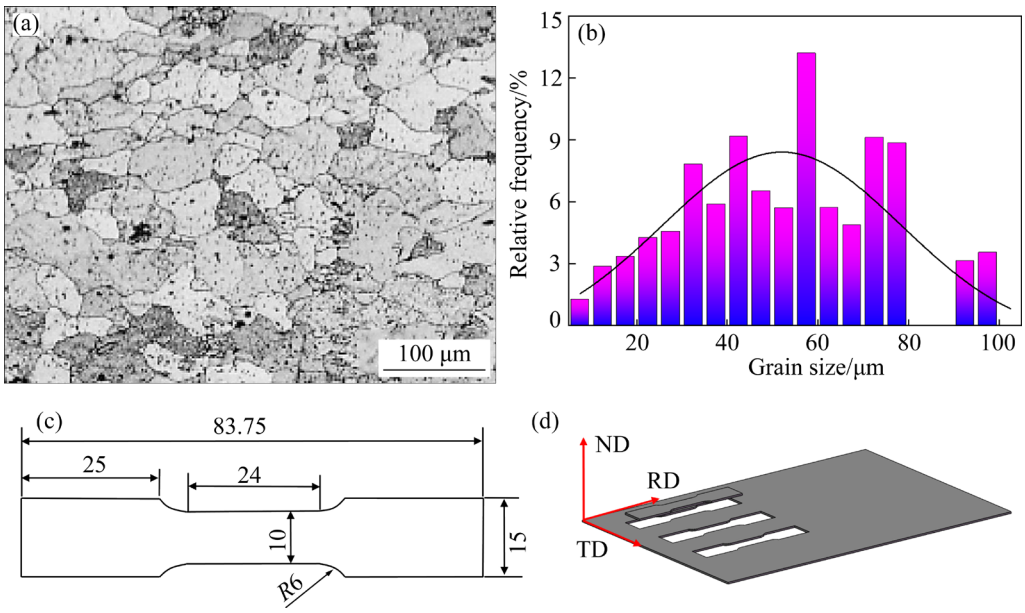

Fig. 1 Basic information of 2195 Al−Li alloy: (a) Initial microstructure; (b) Statistical distribution of grain size; (c) Sample geometry (unit: mm); (d) Cutting method

peaks formed by each precipitated phase and to determine the type and content of precipitated phase. The JEM−2100F transmission electron microscope (TEM) was used to investigate the patterns and morphology of electron diffraction. The yield strength of the 2195 Al−Li alloy was 112 MPa, the tensile strength was 165 MPa, and the elongation after fracture was 16.8%.

2.2 Experimental process

Three process experiments were carried out simultaneously in this work (see Fig. 2). The first process was the HTWD, i.e. the sample was subjected to artificial aging directly after solution treatment. The second process was the TTSF, i.e. the sample after solution treatment was deformed under the stamping forming (SF) loading, and then exposed to artificial aging treatment. The third process was the TTIHF, i.e. the sample after solution treatment was deformed under the IHF loading and then subjected to artificial aging treatment. Impact hydroforming and rigid punch stamping forming can provide different strain rates of metal forming; in the former the strain rate is no less than 10^3 s^{-1}, while in latter it is less than 1 s^{-1}. Based on the current research [31,32], the aging temperatures selected in the study were 165 and 195 °C, respectively. Furthermore, for the sake of clarity, the process routes for three experimental conditions are shown schematically in Fig. 2.

A sample after solid solution treatment is referred to as the solution state; A sample subjected to solid solution treatment and 165 °C artificial peak aging is abbreviated as Aging-AA165; A sample after solution treatment and 195 °C artificial peak aging is abbreviated as Aging-AA195; A sample after solution treatment in the IHF experiment with 10% deformation, and it is abbreviated as the IHF state; The sample after solution treatment is subjected to the SF experiment with 10% deformation, and it is referred to as the SF state; A sample after solution treatment with 10% deformation by IHF and artificial peak aging treatment at 165 °C is abbreviated as IHF10%-Aging-AA165; A sample after solution treatment with 10% deformation by IHF and artificial peak aging treatment at 195 °C is abbreviated as IHF10%-Aging-AA195; A sample after solution treatment with 17% deformation by IHF and artificial peak aging treatment at 195 °C is denoted as IHF17%-Aging-AA195; A sample after solution treatment with 10% deformation by SF and artificial peak aging treatment at 165 °C is abbreviated as SF10%-Aging-AA165; A sample after solution treatment with 10% deformation by SF and artificial peak aging treatment at 195 °C is abbreviated as SF10%-Aging-AA195.

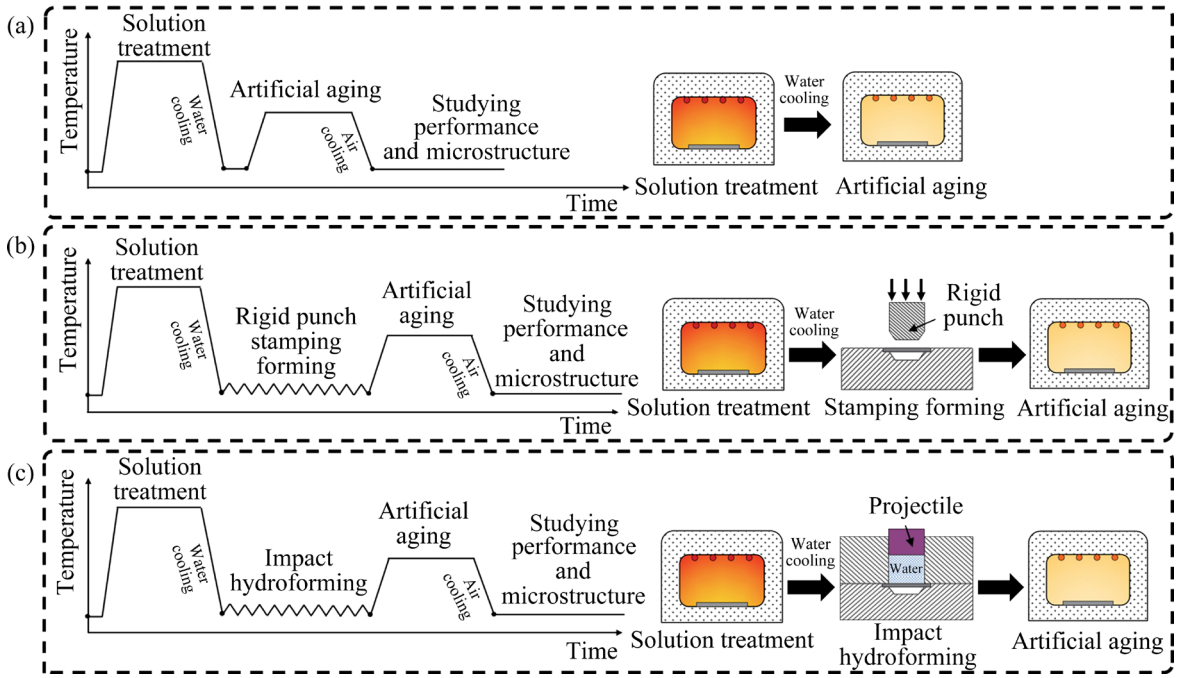

Fig. 2 Schematic diagrams of experimental process routes: (a) HTWD; (b) TTSF; (c) TTIHF

The equipment utilized for IHF primarily consists of a high-pressure power zone, impact projectile acceleration zone, forming zone, and control zone. Before forming, a blank should be covered with plastic wrap to avoid the liquid leakage. The experimental equipment and the die used for IHF deformation are shown in Fig. 3. The experimental equipment of rigid punch stamping is the BCS−50BR hot forming tester for sheet metal, and the experimental equipment and the die used for SF deformation are shown in Fig. 4.

2.3 Control of deformation amount

A crucial aspect of TMT is the precise control of deformation amount. A trapezoidal part (Fig. 5(a)) was designed, which can be used to achieve different deformation amounts by varying the strains and then cutting samples out of the part at the corresponding positions. Various strains of trapezoidal components were achieved by designing five different cavity sizes (Fig. 5(d)). The finite element analysis was used to numerically simulate the equivalent plastic strain at the gauge length that corresponds to the cavity size of the five dies shown in Fig. 5(e). The SF technology is a quasi-static forming process, and a numerical model (Fig. 5(b)) was established for numerical simulation. The IHF is a novel HSR-forming process that involves the joint participation and interaction of fluids and solids [23]. Therefore, it is necessary to develop a solid−liquid coupling finite element (SLC-FE) model (Fig. 5(c)) for numerical simulation. The method of establishing the SLC-FE model is similar to that mentioned in XIA et al [29], so we will not go into details in this the work.

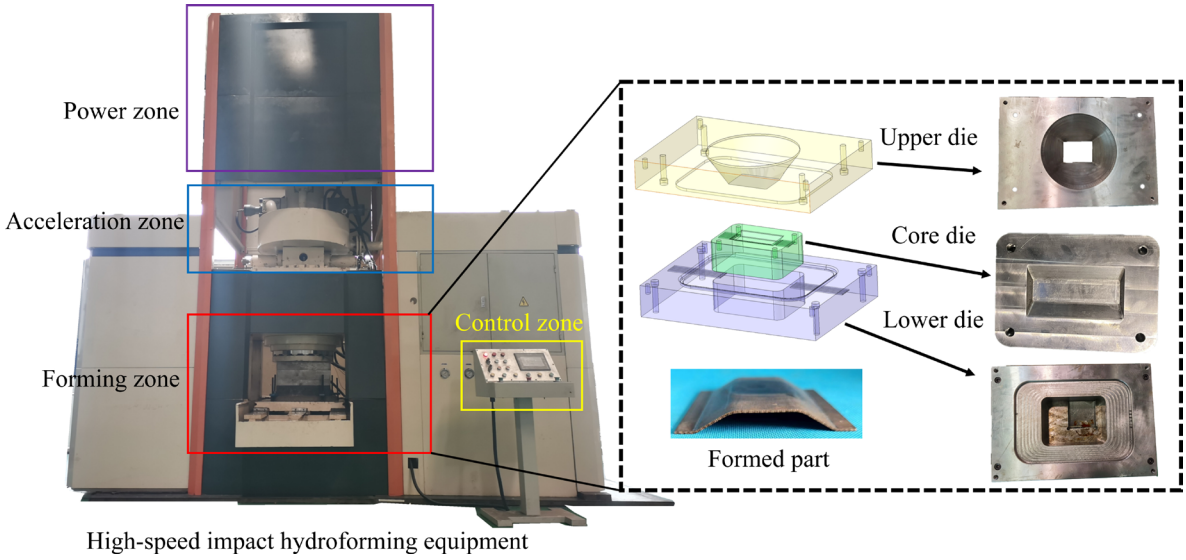

Fig. 3 Equipment and die for IHF deformation

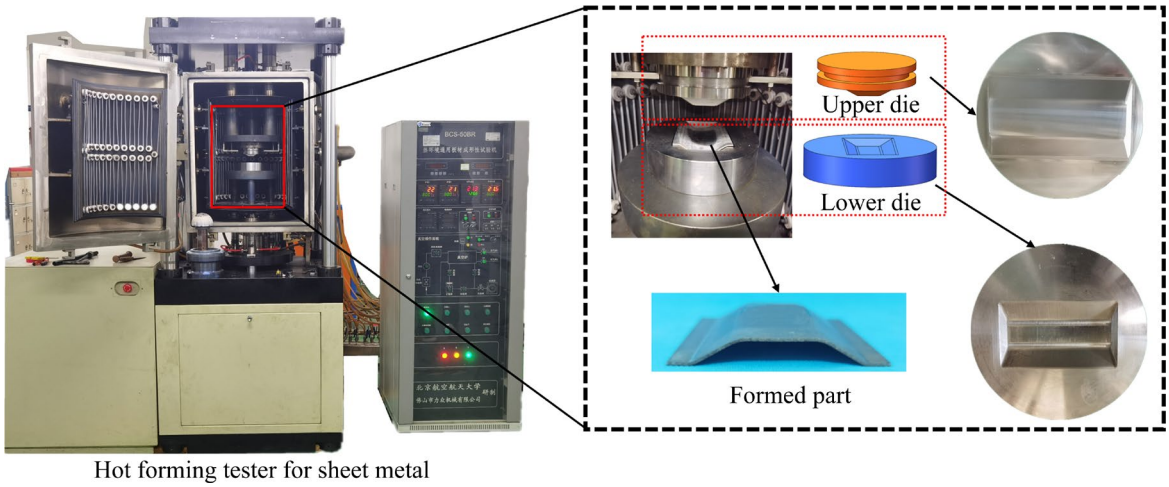

Fig. 4 Equipment and die for SF deformation

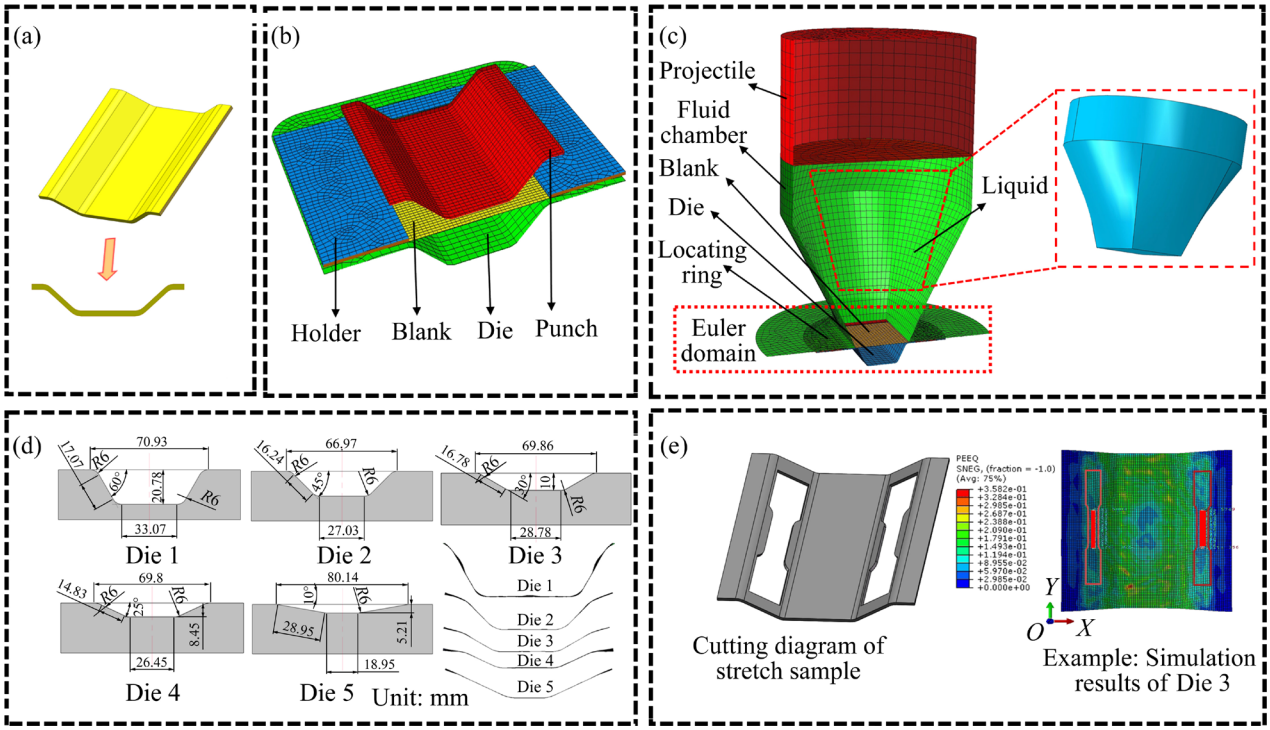

Fig. 5 Methods of deformation control: (a) Trapezoid; (b) SF model; (c) SLC-FE model; (d) 5 cavity sizes and profiles; (e) Die 3 results and sampling locations

Following the experiment, the tensile sample was cut out from the side wall of the part. As an example, the results obtained with Die 3, which is shown in Fig. 5(d), are presented in Fig. 5(e). Meanwhile, the simulation results involve collecting a series of data points at the location where the gauge length of the tensile part is obtained by cutting. The equivalent plastic strain of each point is calculated and the average value is evaluated to reflect the strain at the gauge length in order to guide the subsequent die design. Figure 6 shows the equivalent plastic strain at the gauge length corresponding to different cavity sizes in the simulation results. The average equivalent plastic strain of the gauge length is used to represent the deformation amount. These values for the five cavity sizes under SF are 0.15, 0.10, 0.07, 0.05, and 0.02, respectively. The average equivalent plastic strains for the five cavity sizes under IHF are 0.26, 0.17, 0.13, 0.10, and 0.08, respectively. The average values of 0.10 and 0.17 under SF and IHF are selected, respectively, which guide the subsequent die design. The designed die is used for IHF and SF experiments to analyze the influence of different loading deformation methods on the mechanical properties of 2195 Al−Li alloy.

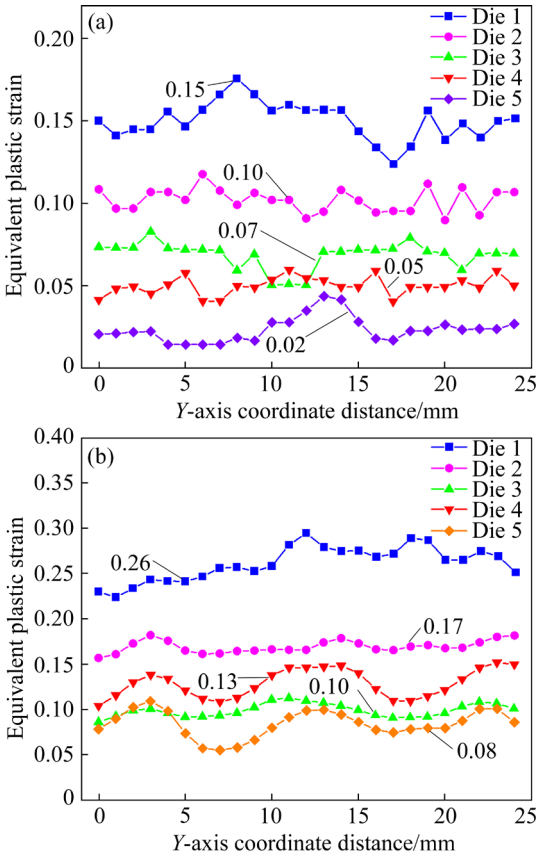

Fig. 6 Equivalent plastic strains at gauge length corresponding to different cavity sizes in simulation results: (a) SF; (b) IHF

3 Results and discussion

3.1 Determination of solution treatment regimes

Solution treatment is a process in which an alloy is heated to a high-temperature single-phase area and held for a certain period, so that the solute atoms are dissolved into the alloy matrix, followed by rapid cooling. The crucial factors of solution treatment are the solution temperature and time. Differential scanning calorimetry (DSC) enables qualitative and quantitative analysis of test materials. The Al−Li alloy was examined using the STA449F3 extreme high-temperature comprehensive thermal analyzer. The results of the DSC test for 2195 Al−Li alloy are displayed in Fig. 7. The graph indicates the presence of two absorption peaks at temperatures of 515 and 652 °C, respectively. The absorption peak at 652 °C corresponds to the melting point of the alloy while the solid solution phase transition temperature of this alloy is 515 °C. The solution temperature is determined by subjecting the solution to a series of treatments within the temperature range from 475 to 555 °C for 90 min, followed by a metallographic examination.

The metallographic micrographs of 2195 Al−Li alloy at different solution temperatures are presented in Fig. 8. When the solid solution treatment temperature is 475 °C (Fig. 8(a)), blocky white structures and a small number of secondary-phase particles in the alloy are observed. When the temperature is 495 °C (Fig. 8(b)), the number of residual crystalline phases decreases, and small pieces of structures are uniformly distributed around the large white structures. At 515 °C (Fig. 8(c)), the residual crystalline phase has mainly dissolved in the Al−Li alloy. At 525 °C (Fig. 8(d)), a remelted ball-shaped fragment and a clear triangular remelted zone appeared at the junction of grain boundaries in the alloy, thus indicating that the alloy is over-burnt. At 535 and 555 °C (Figs. 8(e) and (f)), over-burning is still more obvious. Therefore, to prevent over-burning of the alloy, the solution treatment temperature of 515 °C was selected.

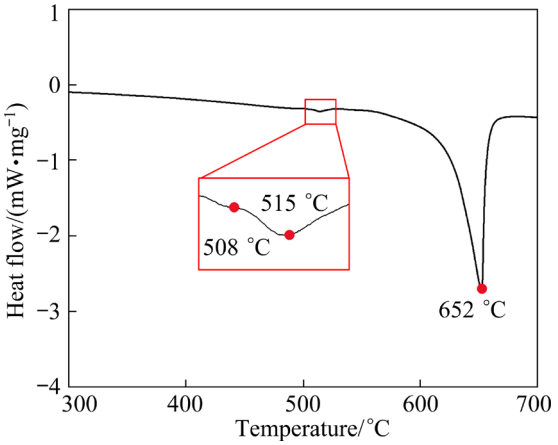

Fig. 7 DSC test results of 2195 Al−Li alloy

To determine the optimal solution time, a series solution treatments were conducted at 515 °C. The corresponding mechanical properties are summarized in Fig. 9. It is seen that both the yield strength and tensile strength of the material initially

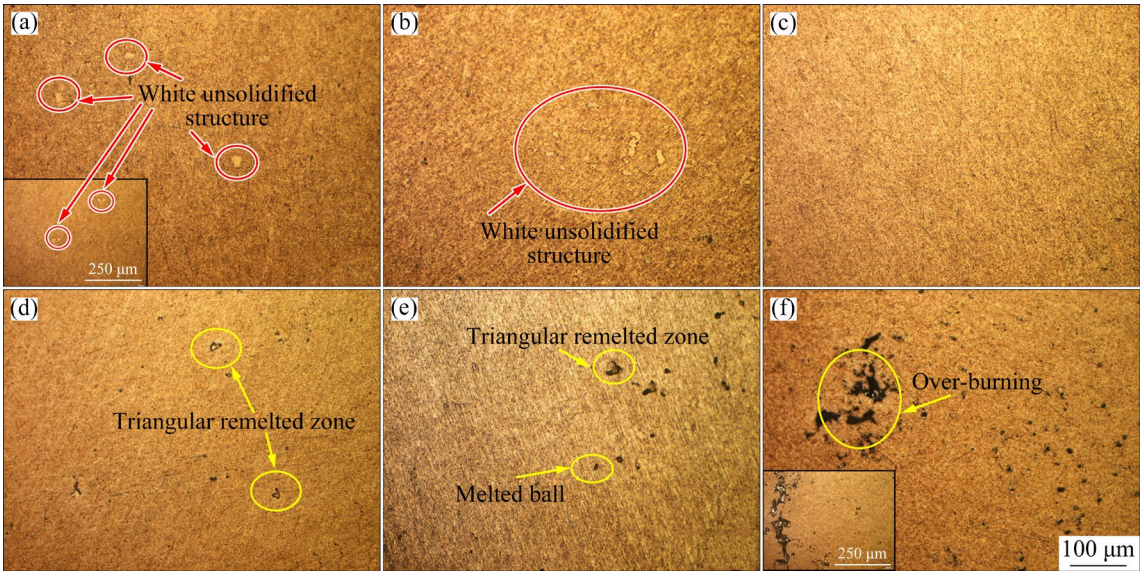

Fig. 8 Metallographic micrographs of 2195 Al−Li alloys at different solution temperatures: (a) 475 °C; (b) 495 °C; (c) 515 °C; (d) 525 °C; (e) 535 °C; (f) 555 °C

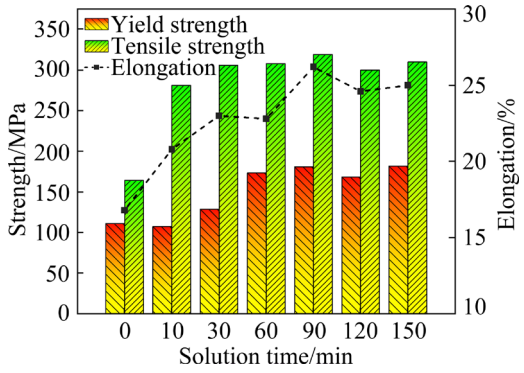

Fig. 9 Mechanical properties of 2195 Al−Li alloys at different solution time

rise and thereafter decline as the solution time increases. At a solution time of 90 min, the yield strength and tensile strength reach their maximum values; 181 MPa and 319 MPa, respectively. With the increase of the solution time, the elongation after fracture of Al−Li alloy first increases and then decreases. When the solution time is 90 min, the highest elongation after fracture of 26.2% is attained. Finally, the treatment parameters are determined as follows: the solution temperature is 515 °C and the time is 90 min.

3.2 Influence of different conditions on peak aging treatment

To investigate the effect of different loading conditions on peak aging, experiments were performed to obtain the hardness variation curves for the 2195 Al−Li alloy under different loading conditions (see Fig. 10). The hardness of the alloy begins to decline slowly after 50 h of artificial aging at 165 °C during the HTWD (Fig. 10(a)); In the case of artificial aging at 195 °C, the alloy hardness starts decreasing after 10 h (Fig. 10(b)). The 2195 Al−Li alloy can reach the peak aging state with the hardness of HV 196 at 165 °C for the exposure time of 50 h. At 195 °C, the peak aging state is reached at 10 h and the corresponding hardness is HV 165. The variations in hardness of the 2195 Al−Li alloy after artificial aging at 165 and 195 °C following TMT under the aforesaid two different conditions exhibit a pattern similar to that of the HTWD.

However, the time required to reach peak aging differs. Under the TMT based on the SF loading deformation with the strain of 10% (TTSF-10%), the 2195 Al−Li alloy can reach a peak aging state at 165 °C after 40 h, which corresponds to a hardness

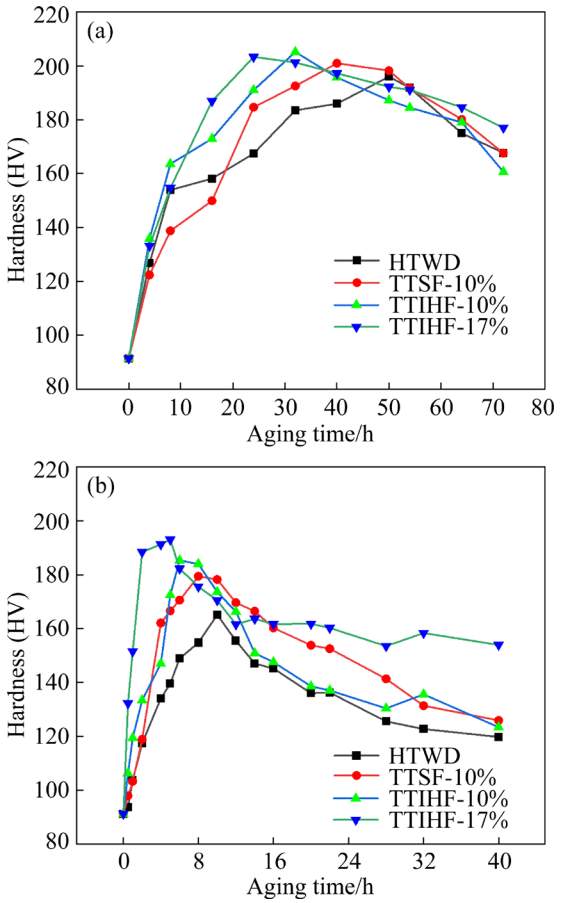

Fig. 10 Hardness curves of 2195 Al−Li alloys under different loading conditions: (a) 165 °C; (b) 195 °C

of HV 200. During the 195 °C aging treatment, the peak aging state is reached after 8 h, with the hardness being HV 179. Under the TMT based on IHF loading with a strain of 10% (TTIHF-10%), the 2195 Al−Li alloy can reach a peak aging state at 165 °C after 32 h, and the corresponding hardness is HV 205. Under the 195 °C aging treatment, the peak aging state with a hardness of HV 185 is reached after 6 h. Under the TMT based on a IHF load with a strain of 17% (TTIHF-17%), the alloy can reach a peak aging state with a hardness of HV 203 after aging treatment at 165 °C for 24 h, while at 195 °C the peak aging state can be reached after 5 h, resulting in a hardness of HV 192.

The results show that compared with HTWD, the time to reach the peak aging state of the 2195 Al−Li alloy is shortened by performing deformation before the aging treatment. If the strains of IHF and SF loading are both 10%, the former demonstrates a shorter time for reaching the peak aging state. With the strain increasing to 17%, the time for reaching the peak aging state is further shortened. In brief,

compared with HTWD, when deformation is used before aging, the time to reach the peak aging state at 165 and 195 °C will be shortened. It is also found that the 2195 Al−Li alloy will have the shortest time to reach the peak aging state when it is treated at higher aging temperatures, but its strength will be slightly lower.

3.3 Effect of different peak aging treatments on mechanical properties

In Fig. 11, the stress−strain curves and mechanical properties of the 2195 Al−Li alloy in different states, which were obtained by using three process routes, are displayed. In Figs. 11(a) and (b), it is seen that under HTWD, the strength and elongation of the alloy after solution treatment are higher than those in the original state, while the strength of the alloy after artificial aging at 165 and 195 °C is further improved. The strength of the alloy after aging at 195 °C is slightly lower than that at 165 °C. In Figs. 11(c) and (d), it is shown that under the TTSF, the strength after SF but without artificial aging is improved as compared to the original and solution states; The yield strength of the SF10%-

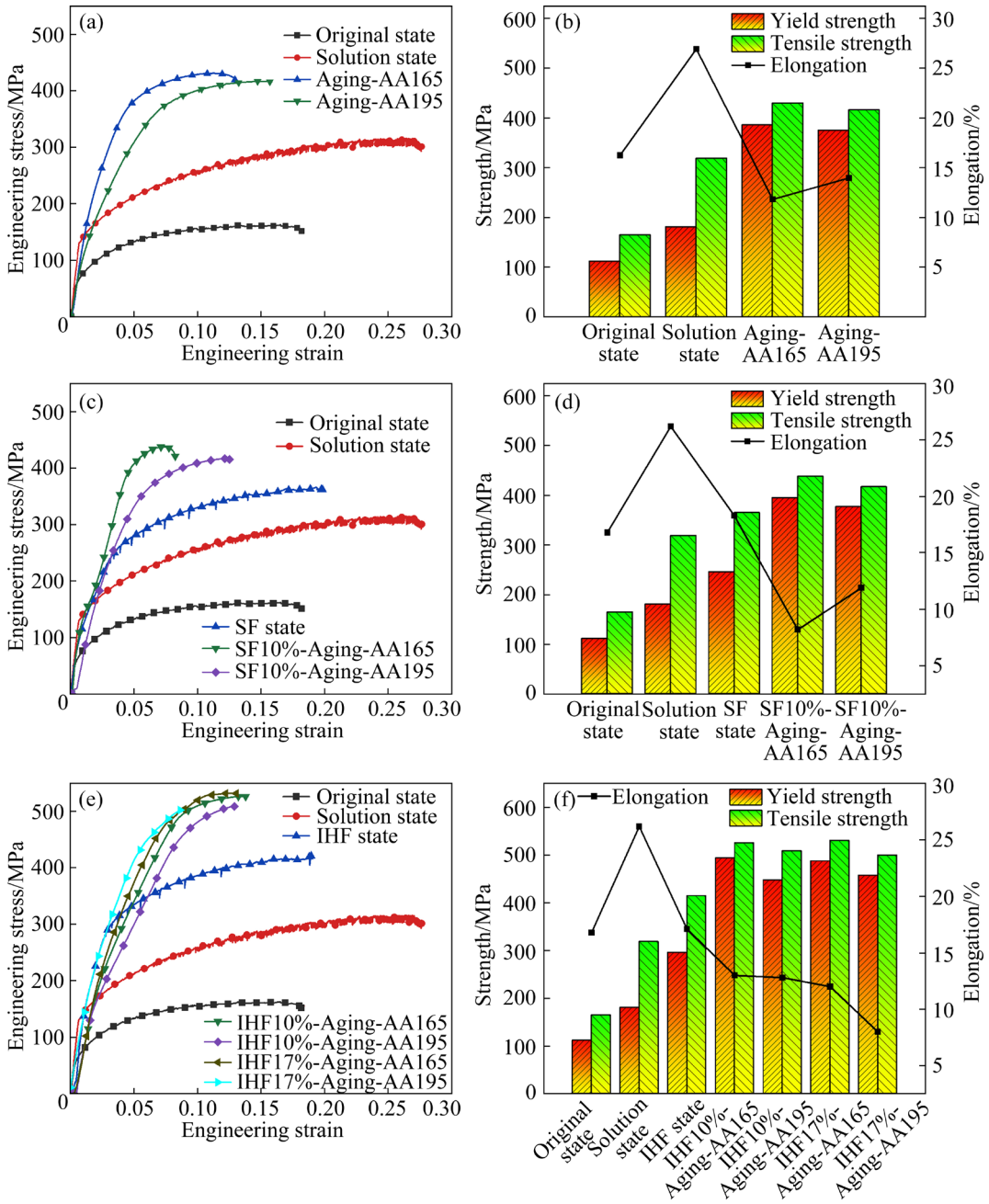

Fig. 11 Stress−strain curves (a, c, e) and mechanical properties (b, d, f) of 2195 Al−Li alloys under different conditions: (a, b) HTWD; (c, d) TTSF; (e, f) TTIHF

Aging-AA165 and SF10%-Aging-AA195 states, i.e. of the samples artificially aged after deformation, is increased by 283 and 265 MPa while the tensile strength is increased by 273 and 252 MPa, respectively, as compared to that of the original state. These findings indicate that TTSF can improve the strength of the 2195 Al−Li alloy. Figures 11(e) and (f) demonstrate that under TTIHF, the strength of the alloy deformed by IHF but without artificial aging is increased as compared with that of the original and solution states. Compared with that of the IHF state, the strength of the alloy after deformation and aging is further improved. Thus, the yield strength of the IHF10%-Aging-AA165 state is increased by 198 MPa, i.e. by 66.8% and the tensile strength is increased by 111 MPa (by 26.7%). This indicates that the TTIHF can substantially enhance strength of the 2195 Al−Li alloy.

To compare the effect of different heat treatments on the mechanical properties more clearly, the data from Figs. 11(b), (d), and (f) are combined in Fig. 12. In comparison with the original and solution states, the strength of the IHF and SF states without artificial aging after deformation is increased, but the strength of the IHF state is higher than that of the SF state. Furthermore, Fig. 12 illustrates that the Al−Li alloy exhibits a higher strength after deformation and artificial aging as compared to heat treatment without deformation. As compared with artificial aging after solution treatment (Aging-AA165), the deformation in the middle of TTSF (SF10%-Aging-AA165) and TTIHF (IHF10%-Aging-AA165) processes improves the strength of Al−Li alloy. After TTIHF, the yield strength of 2195 Al−Li alloy is 491 MPa, which is 18.6% higher than that of TTSF while the tensile strength reaches 518 MPa, which is 18% higher than that of TTSF. Thus, it can be inferred that the TTIHF is more conducive to the strengthening of 2195 Al−Li alloy than the TTSF route. In addition, the mechanical properties under various heat treatments can be compared and analyzed from the red dashed box in Fig. 12. It can be seen that under similar conditions, the strength of the alloy after TTIHF is the highest, and increasing the strain can also improve the strength of the alloy, but the maximum is not more than 15 MPa. Besides, the strength of the alloy after TTSF is slightly higher than that after HTWD.

Through the above analysis, it is shown that: (1) Compared with HTWD, the time to reach the peak aging state of the 2195 Al−Li alloy is shortened by introducing deformation before aging treatment, and this time is the shortest at IHF loading; (2) The strength of the alloy after TTIHF is increased to the highest, and TTIHF is more conducive to the strengthening treatment of the 2195 Al−Li alloy; (3) For the strain of 10% and 165 °C peak aging, the yield strength of 2195 Al−Li alloy after TTIHF is 491 MPa, which is increased by 18.6%, and the tensile strength reaches 518 MPa, which is increased by 18.0% as compared with TTSF; (4) When the strain amounts to 10% and 17%, the strength of the 2195 Al−Li alloy after peak aging at 165 °C under TTIHF is higher than that at 195 °C, but the difference is not significant. When the actual production time is taken into consideration, the optimal heat treatment appears to be artificial aging at 195 °C. On the whole, the TTIHF process is more conducive to the strengthening treatment of 2195 Al−Li alloy than the TTSF, and it can be applied to improving the strength of components made from this material.

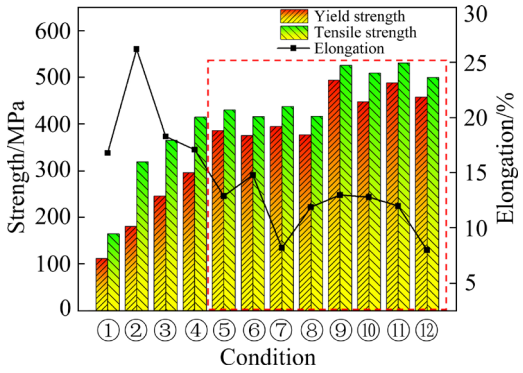

Fig. 12 Comparison of mechanical properties of 2195 Al−Li alloys under different conditions: ① Original state; ② Solution state; ③ SF state; ④ IHF state; ⑤ Aging-AA165; ⑥ Aging-AA195; ⑦ SF10%-Aging-AA165; ⑧ SF10%-Aging-AA195; ⑨ IHF10%-Aging-AA165; ⑩ IHF10%-Aging-AA195; ⑪ IHF17%-Aging-AA165; ⑫ IHF17%-Aging-AA195

3.4 Strengthening mechanism of different peak aging treatments

The TMT procedure involves pre-deforming the alloy before aging, which creates increased dislocation density within the material. Nucleation and growth of the T_1 phase occur at sites with a higher energy such as dislocations and sub-grain boundaries.

Figure 13 presents the transmission electron microscope (TEM) images of the 2195 Al−Li alloy deformed along the $[110]_{Al}$ direction under different loading methods without artificial aging treatment. In Fig. 13(a), the bright field (BF) image of the SF state (deformation at SF loading after solution treatment) is presented, and Fig. 13(b) displays the BF image of the IHF state (deformation under IHF loading after solution treatment). Deformation under both loading methods after solution treatment results in work hardening, so a large number of dislocations are observed in Figs. 13(a) and (b). In Fig. 13, the red circle represents the area where the dislocations are heavily entangled, and the yellow circle indicates the end of dislocations in other directions than $[110]_{Al}$. Different strain rates of the deformation of the TTSF and the TTIHF lead to different numbers of dislocations generated in the alloy. By comparing the results of these two types of loading, it is found that the dislocation density in the BF image of IHF deformation is larger than that in the BF image of SF deformation and the dislocation entanglement is more obvious, which explains the fact that the yield strength and tensile strength of the 2195 Al−Li alloy in IHF state are significantly higher than those in SF state.

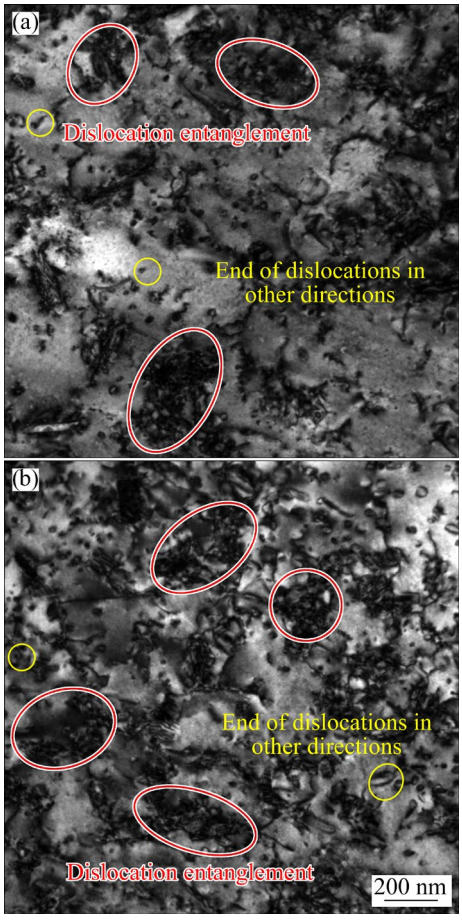

Fig. 13 TEM images of Al−Li alloy under different loading methods without aging: (a) SF; (b) IHF

XU et al [33] found that the deformation time under HSR is short and hence is not sufficient for the rearrangement and partial annihilation of closely spaced dislocations in aluminum alloys. In addition, an increase in the density of movable dislocations under HSR can also lead to a certain degree of the entanglement and accumulation of dislocations. At the same time, HSR loading occurs under the effect of an instantaneous high stress. In such conditions, a local stress in hard-oriented grains exceeds the critical shear stress value, thereby activating slip systems in hard-oriented grains and causing plastic deformation of the latter. This provides a lot of spaces for the proliferation and movement of active dislocations, so that the dislocation distribution becomes more uniform. Mobile dislocations in hard-oriented grains can tangle and accumulate, which results in "secondary hardening" during the deformation stage of the aluminum alloys. This is also consistent with the well-known fact that the dislocation density generated by HSR deformation is much higher than that by LSR deformation [34]. Since dislocations can provide nucleation sites for the precipitation of the T_1 phase in the subsequent artificial aging process, and a high density of dislocations created by deformation during IHF result in a larger number of T_1 phases precipitated in the subsequent aging process as compared with the TTSF, and their distribution is more uniform.

TEM investigation is limited to observing small-scale microstructure. Therefore, XRD was employed to assess the dislocation density on a larger scale. XRD analysis was performed for the 2195 Al−Li alloy in both SF and IHF states (seen Fig. 14). The Williamson−Hall model was used to calculate the dislocation density. The XRD data were put into Jade software to analyze and calculate the full width at half maximum (FWHM) of the alloy. The Williamson−Hall formula [35,36] is as follows:

$$\beta\cos\theta=\frac{k\lambda}{d}+4\varepsilon\sin\theta \tag{1}$$

where β is the full width at half maximum (FWHM) of the alloy, k is a constant, λ is the wavelength of Cu K_α radiation, d is the average grain size, ε is the micro-strain, and θ is the Bragg angle. The $\beta\cos\theta$ and $4\sin\theta$ values obtained by Jade software are plotted in Fig. 15, and the slopes of the two linear

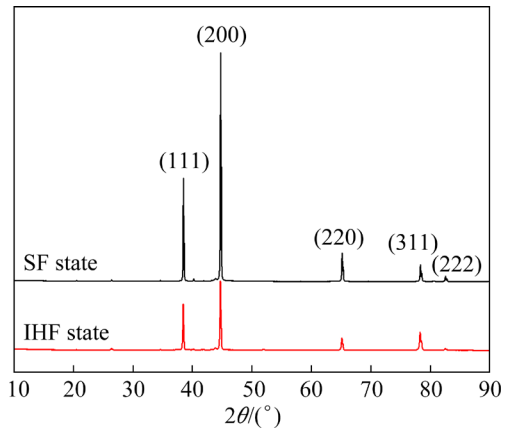

Fig. 14 XRD patterns of 2195 Al−Li alloy in SF and IHF states

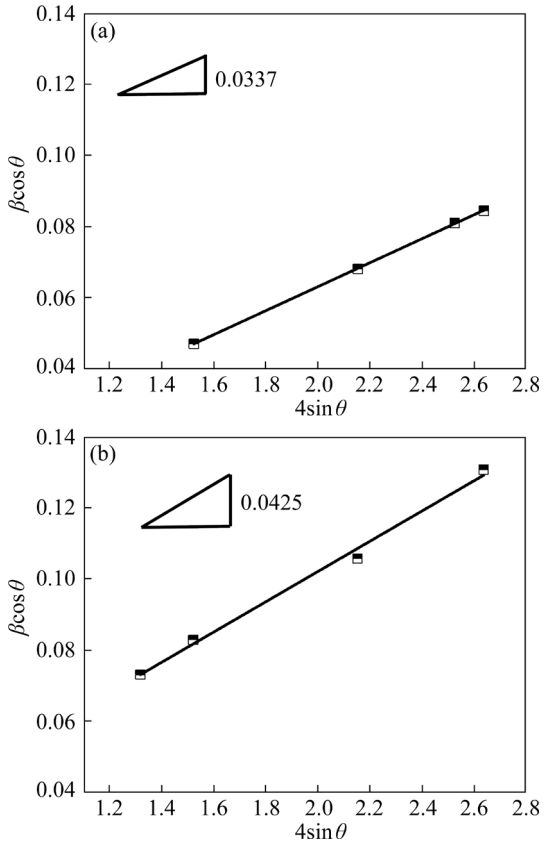

Fig. 15 $\beta\cos\theta$ and $4\sin\theta$ functions of 2195 Al−Li alloy: (a) SF state; (b) IHF state

relations are obtained to reveal that the micro-strain ε for SF and IHF states are 0.0337 and 0.0425, respectively. The average grain size (d) appears to be 52.28 μm. The dislocation density (ρ) can be calculated by Eq. (2) as follows:

$$\rho=\frac{2\sqrt{3}\varepsilon}{db} \tag{2}$$

where b is the magnitude of Burgers vector (for aluminum alloys, b=0.289 nm [37]). The dislocation densities of 2195 Al−Li alloys in SF and IHF states are 7.68×10^{13} and 9.69×10^{13} m^{-2}, respectively. The dislocation density of the alloy under IHF loading is higher than that under SF loading, which is consistent with the TEM results.

The TEM analysis of the 2195 Al−Li alloy after TMT with different loading methods was carried out. BF images of 2195 Al−Li alloy in different states along the $[110]_{Al}$ direction and their corresponding selected area electron diffraction (SAED) patterns are shown in Figs. 16(a) and (b), correspondingly, for Aging-AA165 specimens. Weak diffraction spots and stripes of the T_1 phase are observed in the SAED pattern along the $[110]_{Al}$ direction, and T_1 phase precipitates can be observed in the BF image. The diffraction spots of θ' and δ' phases are not seen in the SAED pattern, but a certain amount of θ' phase and a small amount of δ' phase precipitates can be observed in the BF image. Figures 16(c) and (d) show the BF image and SAED pattern of SF10%-Aging-AA165, respectively. Weak diffraction spots and stripes of the T_1 phase are observed in the SAED pattern along the $[110]_{Al}$ direction. The T_1 phases of SF10%-Aging-AA165 can be seen in the BF image, and they are more numerous than those of Aging-AA165. The diffraction spots of the θ' phase are not observed in the SAED pattern, but a small amount of θ' precipitated phase is noticed in the BF image. Compared with Fig. 16(a), it can be seen that the number of θ' phases decreases while the number of T_1 phases increases. This phenomenon indicates that a decrease in the number of θ' phases occurs during pre-deformation before aging, and the precipitates are mainly the T_1 phase with uniform distribution. Figures 16(e) and (f) display the BF image and SAED pattern of IHF10%-Aging-AA165, respectively. Diffraction spots and stripes of the T_1 phase are observed in the SAED patterns along the $[110]_{Al}$ direction. The BF image exhibits a significant quantity of the T_1 phase. Compared with Aging-AA165 and SF10%-Aging-AA165, the number density of the precipitated T_1 phase increases for IHF10%-Aging-AA165, and features a more uniform distribution and smaller size. A small number of θ' phases can be observed in the BF image, but their amount is relatively small as compared to Figs. 16(a) and (c).

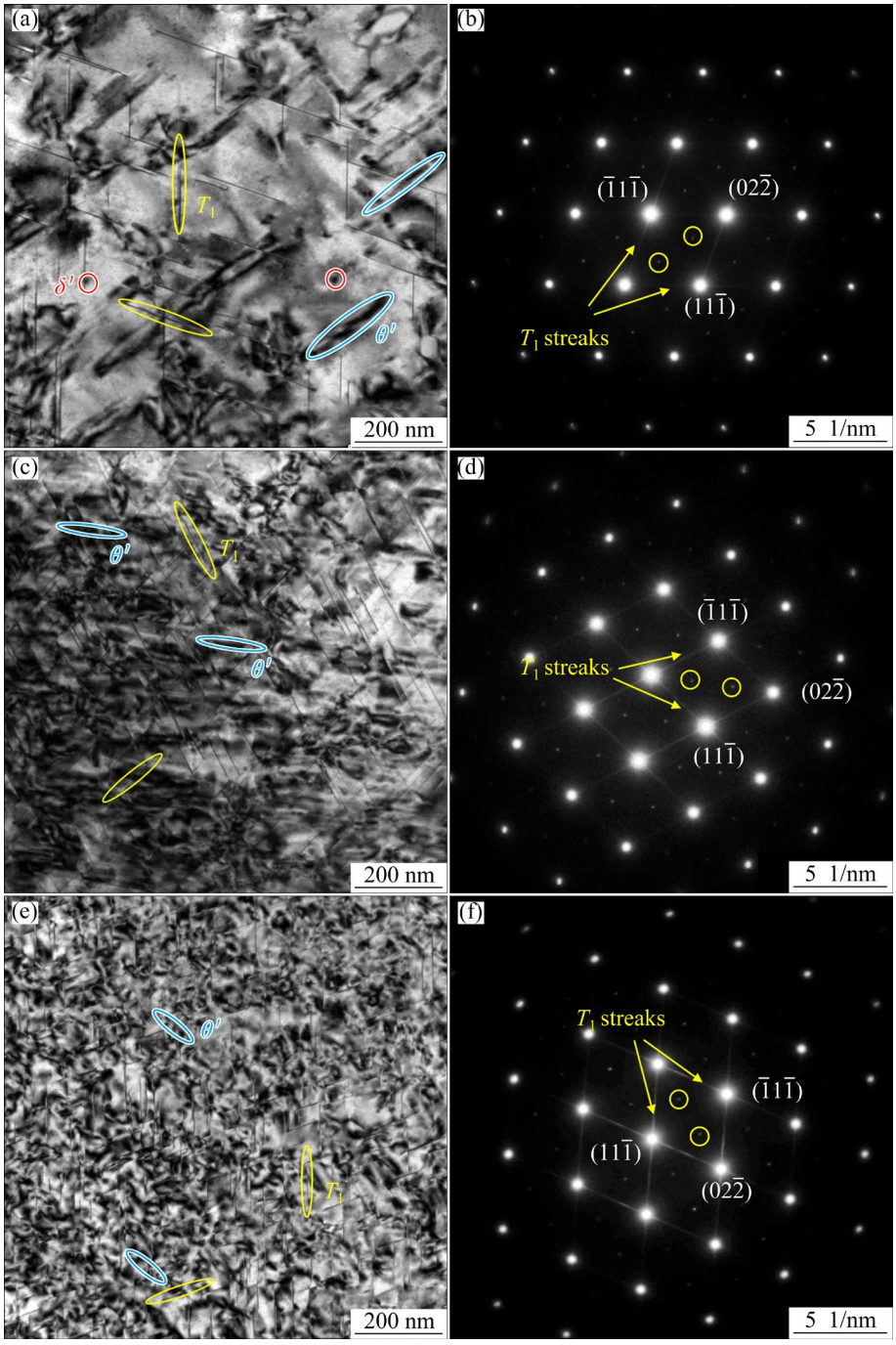

Fig. 16 TEM images (a, c, e) and SAED patterns (b, d, f) of 2195 Al−Li alloys in different states: (a, b) Aging-AA165; (c, d) SF10%-Aging-AA165; (e, f) IHF10%-Aging-AA165

Since the T_1 phase is an equilibrium phase and θ' phase is a metastable phase, a change in the volume free energy required to form the T_1 phase is higher than that required to form the θ' phase. A relatively high volume free energy change associated with the T_1 and the {111} shear strain energy can promote the nucleation of the T_1 phase on the matrix dislocations in preference to that of θ' phase. Meanwhile, the dislocation generated by deformation may become a defect of vacancy annihilation, which reduces the number of vacancies, inhibits the precipitation of the θ' phase and promotes precipitation of the T_1 phase [38]. Deformation in TMT results in a high-density dislocations, which provides a significant number of nucleation sites for the T_1 phase. Additionally, this process consumes the atoms necessary for the cubic phase, hence substantially restricting the precipitation of the latter.

During the middle and later stages of aging, the formation of the T_1 phase consumes θ' and δ phases. In the TTIHF conditions, the number of T_1 phases precipitated in the 2195 Al−Li alloy is the highest and their distribution is the most uniform.

The T_1 phase, which acts as a primary strengthening precipitate, can reduce the coplanar slip and greatly enhance the strength of the alloy. Statistical analysis was performed to evaluate the T_1-phase diameter in the BF images of Figs. 16(a), (c), and (e) for three different situations: Aging-AA165, SF10%-Aging-AA165 and IHF10%-Aging-AA165, respectively. The results of this analysis are presented in Fig. 17. The average diameters for these

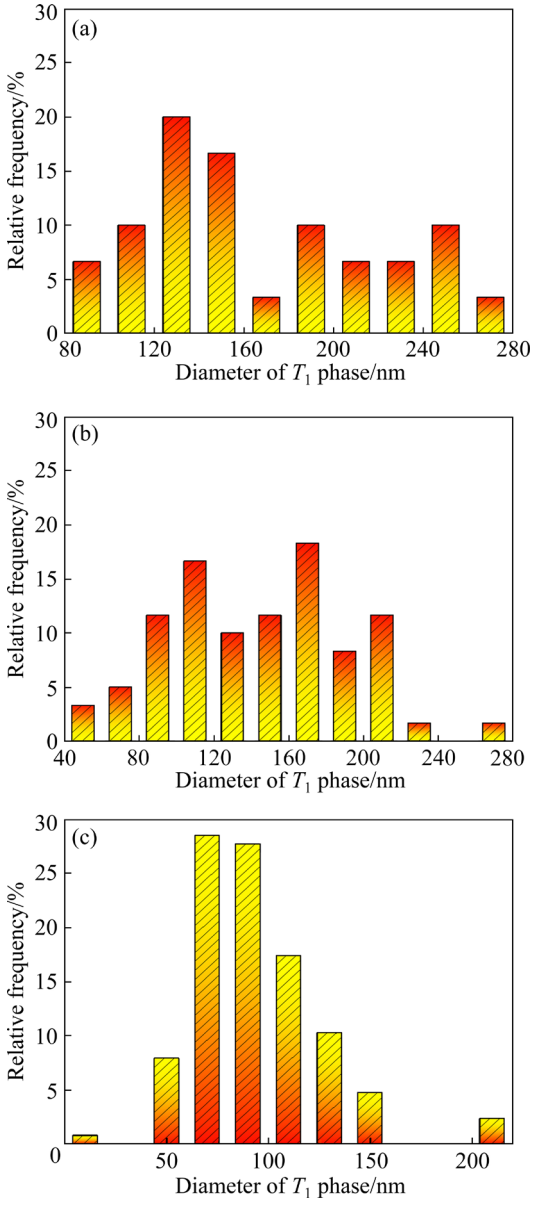

Fig. 17 Statistics of T_1 phase diameter of 2195 Al−Li alloy in different states: (a) Aging-AA165; (b) SF10%-Aging-AA165; (c) IHF10%-Aging-AA165

cases are 159.96, 144.63, and 93.31 nm, respectively, i.e. the diameter of the T_1 phase precipitated under the condition of IHF10%-Aging-AA165 is the smallest.

From the above results, it can be seen that the amount of T_1 phase precipitated in the Al−Li alloy under SF10%-Aging-AA165 and IHF10%-Aging-AA165 conditions is larger than that under Aging-AA165. Under IHF10%-Aging-AA165 condition, the T_1 phase has the maximum number density, the most uniform distribution and the smallest diameter. The dense distribution of the T_1 phases hinders the dislocation movement and requires a larger tensile stress to cause plastic deformation of the alloy, which seems to be the reason for the highest strength of the 2195 Al−Li alloy after TTIHF.

DORIN et al [39], and RODGERS and PRANGNELL [40], based on the interaction mechanism between the T_1 phase and dislocations, assumed that the volume fraction of the phase is constant, and established Eq. (3) as a functional relationship between the number density and size of the T_1 phase and precipitation strengthening ($\Delta\sigma$).

$$\Delta\sigma \propto D^2 N^{1/2} t^{-3/2} \tag{3}$$

The T_1 phase is characterized by a diameter D, number density N and thickness t. According to Eq. (3), D and N are directly proportional to the precipitation strengthening, while t is inversely proportional to the strengthening. The results show that the strengthening effect of the T_1 phase is proportional to the ratio of diameter to thickness, and the strengthening effect is reduced when the thickness of the T_1 phase is too large. Consequently, the more uniform the distribution of the T_1 phase is, the smaller its thickness is, and the higher the strength of the alloy is [35,41].

In Fig. 18, the high-resolution TEM images of Aging-AA165, SF10%-Aging-AA165 and IHF10%-Aging-AA165 are displayed. The T_1 phases grow along the $\{111\}_{Al}$ plane. There are distinct and well-defined boundaries at the interface between the T_1 phase and the Al matrix. In Fig. 18, it is seen that the thickness of the T_1 phase for the three states are 2.82, 2.46 and 1.29 nm, respectively. These indicate that deformation has a significant effect on the T_1 phase precipitates. After the TTIHF, the T_1 phases precipitated from the 2195 Al−Li alloy have not only the largest number density and the most uniform distribution but also the smallest thickness, which

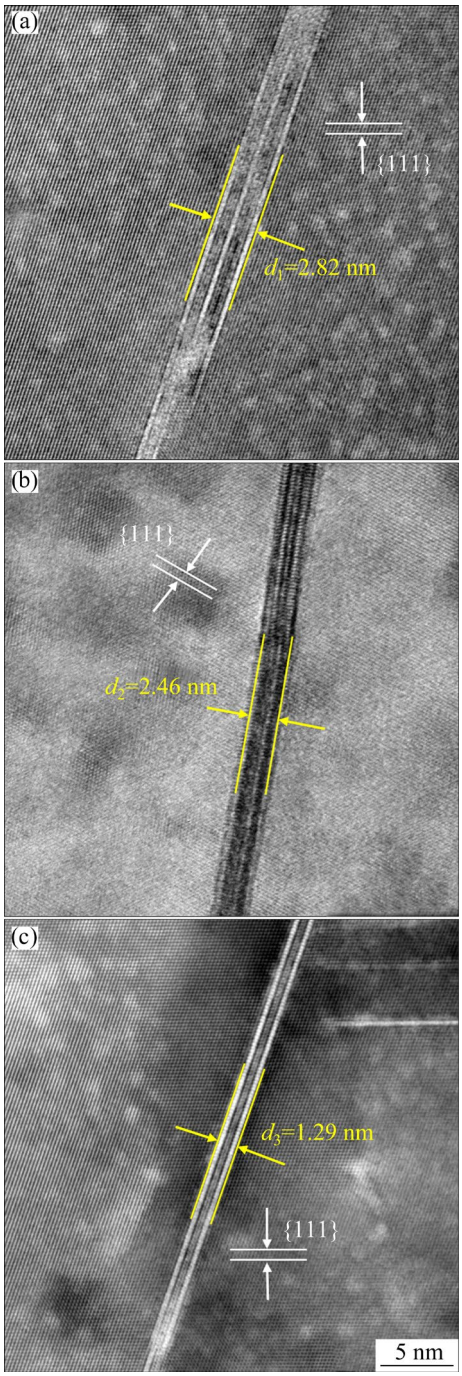

Fig. 18 High-resolution TEM images of aged 2195 Al−Li alloy in different states: (a) Aging-AA165; (b) SF10%-Aging-AA165; (c) IHF10%-Aging-AA165

further explains that this alloy has the highest strength after TTIHF.

In summary, it should be noted that the deformation processes of TTIHF and TTSF can generate a large number of dislocations before aging. An increased dislocation density enhances the formation of nucleation sites for the T_1 phase and facilitates its precipitation. The movement of dislocations is hindered and pinned by the precipitated phase. Therefore, the strength of the alloy is improved by the deformation before aging. Among, the IHF loading deformation with high dislocation density in the subsequent aging process brings about a larger amount of precipitated T_1 phases compared to the SF loading deformation. Additionally, the distribution of the T_1 phase in the former case is more uniform and the particles are finer. The obtained results indicate that the TTIHF process is more efficient for improving the strength of the 2195 Al−Li alloy than TTSF, and the strengthening effect is still more significant after the subsequent aging treatment. Hence, the TTIHF process exhibits a good prospect for the promotion and application.

4 Conclusions

(1) The peak aging treatments of TTIHF of the 2195 Al−Li alloy are as follows: when the strain is 10%, they are 165 °C for 32 h and 195 °C for 6 h. When the strain is 17%, they are 165 °C for 24 h and 195 °C for 5 h. In comparison with HTWD and TTSF, the peak aging time of the alloy under TTIHF is shortened substantially.

(2) For the case when the strain is 10% and the temperature is 165 °C, the TTIHF process appears more efficient for strengthening the 2195 Al−Li alloy than TTSF. The yield strength and tensile strength of the 2195 Al−Li alloy are 491 and 518 MPa after TTIHF, which are 18.6% and 18.0% higher than those for TTSF.

(3) Both the IHF and SF loading methods introduce dislocations into the alloy. The comparative study has demonstrated that the dislocation generated by IHF is higher than that in the case of SF, the dislocation entanglement is obvious, and the dislocation densities are 9.69×10^{13} and 7.68×10^{13} m^{-2}, respectively. The dislocations provide nucleation sites for the precipitation of the T_1 phase during the subsequent artificial aging, and a high dislocation density is conducive to increasing the amount of the T_1 phases.

(4) Compared with HTWD and TTSF, the number density, size and distribution of the T_1 phase in the alloy after TTIHF are the largest, the smallest and the most uniform, respectively. The uniformly distributed fine T_1 phase hinders the movement of dislocations, which requires a higher stress to plastic

deformation of the alloy. This provides an explanation to the observed fact that the 2195 Al−Li alloy demonstrates the highest strengthening effect after TTIHF.

CRediT authorship contribution statement

Hong-liang ZHU: Methodology, Investigation, Data curation, Writing − Reviewing & editing; **Yong XU:** Conceptualization, Funding acquisition, Writing − Reviewing & editing; **Wen-long XIE:** Methodology, Conceptualization, Funding acquisition, Writing − Reviewing & editing; **Shi-hong ZHANG:** Conceptualization, Supervision, Funding acquisition, Writing − Reviewing & editing; **Xiu-wen LV:** Writing − Reviewing & editing, Resources; **Muhammad Farooq SALEEM:** Writing – Reviewing & editing, Resources; **Artur I. POKROVSKY:** Writing – Reviewing & editing, Resources; **Boris B. KHINA:** Writing – Reviewing & editing, Resources.

Declaration of competing interest

The authors declare that they have no known competing financial interests or personal relationships that could have appeared to influence the work reported in this paper.

Acknowledgments

This study was financially supported by the National Key R&D Program of China (Nos. 2024YFE0108800, T24KITG-014), and the International Partnership Program of Chinese Academy of Sciences (No. 172GJHZ2022096FN).

References

[1] EL-ATY A A, XU Yong, ZHANG Shi-hong, HA Sang-yul, MA Yan, CHEN Da-yong. Impact of high strain rate deformation on the mechanical behavior, fracture mechanisms and anisotropic response of 2060 Al−Cu−Li alloy [J]. Journal of Advanced Research, 2019, 18: 19−37.

[2] EL-ATY A A, HA Sang-yul, HOU Yong, XU Yong, ZHANG Shi-hong, XIA Liang-liang, AHMED M Z. Characterization and constitutive analysis-based crystal plasticity of warm flow and fracture behaviours of 2060 Al−Cu−Li alloy [J]. Journal of Materials Research and Technology, 2023, 26: 1624−1648.

[3] ZHANG Qing-you, ZHANG Cun-sheng, LIN Jun, ZHAO Guo-qun, CHEN Liang, ZHANG Hao. Microstructure analysis and low-cycle fatigue behavior of spray-formed Al−Li alloy 2195 extruded plate [J]. Materials Science and Engineering: A, 2019, 742: 773−787.

[4] EL-ATY A A, XU Yong, GUO Xun-zhong, ZHANG Shi-hong, MA Yan, CHEN Da-yong. Strengthening mechanisms, deformation behavior, and anisotropic mechanical properties of Al−Li alloys: A review [J]. Journal of Advanced Research, 2017, 10: 49−67.

[5] IVANOV R, DESCHAMPS A, de GEUSER F D. High throughput evaluation of the effect of Mg concentration on natural ageing of Al−Cu−Li−(Mg) alloys [J]. Scripta Materialia, 2018, 150: 156−159.

[6] EL-ATY A A, XU Yong, ZHANG Shi-hong, MA Yan, CHEN Da-yong. Experimental investigation of tensile properties and anisotropy of 1420, 8090 and 2060 Al−Li alloys sheet undergoing different strain rates and fibre orientation: a comparative study [J]. Procedia Engineering, 2017, 207: 13−18.

[7] ZHANG Xue-song, CHEN Yong-jun, HU Jun-ling. Recent advances in the development of aerospace materials [J]. Progress in Aerospace Sciences, 2018, 97: 22−34.

[8] ZHU Lei, LI Nan, CHILDS P R N. Light-weighting in aerospace component and system design [J]. Propulsion and Power Research, 2018, 7(2): 103−119.

[9] WILLIAMS J C, STARKE E A. Progress in structural materials for aerospace systems [J]. Acta Materialia, 2003, 51(19): 5775−5799.

[10] HAJJIOUI E A, BOUCHAÂLA K, FAQIR M, ESSADIQI E. A review of manufacturing processes, mechanical properties and precipitations for aluminum lithium alloys used in aeronautic applications [J]. Heliyon, 2023, 9(3): e12565.

[11] XIE Bing-xin, HUANG Liang, XU Jia-hui, WANG Yu, XU Yi-ke, ZHANG Hui-ping, LI Jian-jun. Deformation behavior and formability of solid solution state Al−Li alloy in electromagnetic forming [J]. Materials Science and Engineering: A, 2022, 854: 143858.

[12] ZHEN Liang, CUI Yue-xian, SHAO Wen-zhu, YANG De-zhuang. Deformation and fracture behavior of a RSP Al−Li alloy [J]. Materials Science and Engineering: A, 2002, 336(10): 135−142.

[13] GAO Chong, LUAN Yang, YU Jun-chuan, MA yue. Effect of thermo-mechanical treatment process on microstructure and mechanical properties of 2A97 Al−Li alloy [J]. Transactions of Nonferrous Metals Society of China, 2014, 24(7): 2196−2202.

[14] CASSADA W A, SHIFLET G J, STARKE E A. Mechanism of Al_2CuLi (T_1) nucleation and growth [J]. Metallurgical Transactions A, 1991, 22: 287−297.

[15] NOBLE B, THOMPSON G E. T_1 (Al_2CuLi) precipitation in aluminium−copper−lithium alloys [J]. Metal Science Journal, 1972, 6: 167−174.

[16] XIE Bing-xin, HUANG Liang, XU Jia-hui, SU Hong-liang, ZHANG Hui-ping, XU Yi-ke, LI Jian-jun, WANG Yu. Effect of the aging process and pre-deformation on the precipitated phase and mechanical properties of 2195 Al−Li alloy [J]. Materials Science and Engineering: A, 2022, 832: 142394.

[17] CHEN Xiao-xue, ZHAO Guo-qun, XU Xiao, WANG Yong-xiao. Effects of heat treatment on the microstructure, texture and mechanical property anisotropy of extruded 2196 Al−Cu−Li alloy [J]. Journal of Alloys and Compounds, 2021, 862: 158102.

[18] LI Shi-yong, WANG Qi, CHEN Jiang-hua, WU Cui-lan. The effect of thermo-mechanical treatment on the formation of T_1 phase and $\delta'/\theta'/\delta$ composite precipitate in an Al−Cu−Li−Mg

alloy [J]. Materials Characterization, 2021, 176: 111123.

[19] LI Xi-feng, LEI Kun, SONG Peng, LIU Xin-qin, ZHANG Fei, LI Jian-fei, CHEN Jun. Strengthening of aluminum alloy 2219 by thermo-mechanical treatment [J]. Journal of Materials Engineering and Performance, 2015, 24(10): 3905−3911.

[20] XU Jia-hui, HUANG Liang, XIE Bing-xin, LI Jian-jun. Processing and performance of electromagnetic deformation combined with heat treatment of 2195 Al−Li alloy [J]. IOP Conference Series: Materials Science and Engineering, 2022, 1270: 012019.

[21] YAN Si-liang, YANG He, LI Hong-wei, YAO Xuan. A unified model for coupling constitutive behavior and micro-defects evolution of aluminum alloys under high-strain-rate deformation [J]. International Journal of Plasticity, 2016, 85: 203−229.

[22] XIE Bing-xin, HUANG Liang, XU Jia-hui, WANG Yu, LI Jian-jun. Microstructure evolution and strengthening mechanism of Al−Li alloy during thermo-electromagnetic forming process [J]. Journal of Materials Processing Technology, 2023, 315: 117922.

[23] ZHU Hong-liang, XU Yong, CHEN Shuai-feng, ZHANG Shi-hong. Effect of blank size on impact hydroforming of 2195 Al−Li alloy half-tube part with curvature [J]. IOP Conference Series: Materials Science and Engineering, 2023, 1284: 012024.

[24] ZHANG Shi-hong, LI Hao, XU Yong, CHEN Shuai-feng, SONG Hong-wu. Formability and spring-back of light metals at high strain rates [C]//Proceedings of the 14th International Conference on the Technology of Plasticity. Cham: Springer, 2024: 571−578.

[25] CHEN Da-yong, XU Yong, ZHANG Shi-hong, MA Yan, EL-ATY A A, BANABIC D, POKROVSKY A I, BAKINOVSKAYA A A. A novel method to evaluate the high strain rate formability of sheet metals under impact hydroforming [J]. Journal of Materials Processing Technology, 2021, 287: 116553.

[26] AZARYAN N S, SHIRKOV G D, ZHURAUSKI A Y, PETRAKOVSKI V S, BATOURITSKI M A. Manufacture of superconducting niobium cavity parts by hydropercussion punching [J]. Physics of Particles and Nuclei Letters, 2016, 13(2): 218−223.

[27] AKST O, DJAKOW E, HOMBERG W. Some aspects regarding the use of a pneumomechanical high speed forming process [C]//Proceedings of the 5th International Conference on High Speed Forming. Dortmund: Dortmund Technische Universität, 2012: 23−31.

[28] HOMBERG W, DJAKOW E, DAMEROW O. Process reliability and reproducibility of pneu-momechanical and electrohydraulic forming processes [C]//Proceedings of the 6th International Conference on High Speed Forming. Dortmund: Dortmund Technische Universität, 2014: 217−228.

[29] XIA Liang-liang, ZHANG Shi-hong, XU Yong, CHEN Shuai-feng, KHINA B B, POKROVSKY A I. Deformation characteristics and inertial effect of complex aluminum alloy sheet part under impact hydroforming: experiments and numerical analysis [J]. Advances in Manufacturing, 2023, 11: 311−328.

[30] LI Hao, XIE Si-rui, ZHANG Shi-hong, CHEN Shuai-feng, SONG Hong-wu, XU Yong, POKROVSKY A I, KHINA B B. Spring-back behaviors of Ti−6Al−4V sheet under effect of strain rate [J]. International Journal of Mechanical Sciences, 2023, 260: 108646.

[31] GAO Wen-li, YAN Hao, FENG Zhao-hui, LU Zheng. Effect of aging treatment on microstructure and mechanical properties of 2A97 Al−Li alloy [J]. The Chinese Journal of Nonferrous Metals, 2014, 24(5): 1206−1211. (in Chinese)

[32] LI Hong-ying, ZHANG Xiao-jun, ZHANG Jian-fei, ZHENG Zi-qiao. Effect of multi-stage ageing treatments on microstructures and mechanical properties of new-type Al−Cu−Li alloy [J]. The Chinese Journal of Nonferrous Metals, 2008, 18(3): 426−432. (in Chinese)

[33] XU Yong, XIA Liang-liang, EL-ATY A A, XIE Wen-long, CHEN Shuai-feng, KHINA B B, POKROVSKY A I, ZHANG Shi-hong. Revealing the dynamic behavior and micromechanisms of enhancing the formability of AA1060 sheets under high strain rate deformation [J]. Journal of Materials Research and Technology, 2024, 28: 2402−2409.

[34] JIN Yan-ye, YU Hai-ping. Superior mechanical properties and microstructual evolution of 2195-T6 Al−Li alloys at a high strain rate [J]. Materials Science and Engineering A, 2021, 816: 141314.

[35] WILLIAMSON G K, SMALLMAN R E. Dislocation densities in some annealed and cold-worked metals from measurements on the X-ray Debye−Scherrer spectrum [J]. The Philosophical Magazine, 1956, 1(1): 34−46.

[36] WU Ya-ke, LI Ya, LU Jun-yong, TAN Sai, JIANG Feng, SUN Jun. Correlations between microstructures and properties of Cu−Ni−Si−Cr alloy [J]. Materials Science and Engineering: A, 2018, 731: 403−412.

[37] XU Jia-hui, HUANG Liang, XU Yi-ke, XIE Bing-xin, ZHAO Ming-jie, SU Hong-liang, WANG Yu, LI Jian-jun. Effect of pulsed electromagnetic field treatment on dislocation evolution and subsequent artificial aging behavior of 2195 Al−Li alloy [J]. Materials Characterization, 2022, 187: 111872.

[38] WANG Dong-lin, LI Shi-chen, WANG Xiao-ning, ZHENG Zi-qiao. Precipitation of new cubic phase in Al−Li alloys and its mechanism [J]. The Chinese Journal of Nonferrous Metals, 2009, 19(12): 2119−2127. (in Chinese)

[39] DORIN T, DESCHAMPS A, de GEUSER F D, SIGLI C. Quantification and modelling of the microstructure/strength relationship by tailoring the morphological parameters of the T_1 phase in an Al−Cu−Li alloy [J]. Acta Materialia, 2014, 75(11): 134−146.

[40] RODGERS B I, PRANGNELL P B. Quantification of the influence of increased pre-stretching on microstructure−strength relationships in the Al−Cu−Li alloy AA2195 [J]. Acta Materialia, 2016, 108: 55−67.

[41] MA Yun-long, LI Jin-feng. Variation of aging precipitates and mechanical strength of Al−Cu−Li alloys caused by small addition of rare earth elements [J]. Journal of Materials Engineering and Performance, 2017, 26(9): 4329−4339.

冲击液压加载形变热处理 2195 铝锂合金的强化机理

朱红亮[1,2]，徐 勇[1,2]，解文龙[1,2]，张士宏[1,2]，吕秀文[1,2]，Muhammad Farooq SALEEM[1,2]，
Artur I. POKROVSKY[3]，Boris B. KHINA[3]

1. 中国科学院 金属研究所，沈阳 110016；
2. 中国科学技术大学 材料科学与工程学院，沈阳 110016；
3. Physical-Technical Institute, National Academy of Science of Belarus, Minsk 2200084, Belarus

摘 要：提出了一种新型基于冲击液压成形的形变热处理方法(TTIHF)。预变形采用冲击液压成形(IHF)加载实现。研究了 2195 铝锂合金在不同加载预变形条件下的强化效果及机理。结果表明：经 TTIHF 处理后合金达到峰时效的时间缩短。与冲压预变形铝锂合金性能相比，经 TTIHF 处理后铝锂合金的屈服强度和抗拉强度分别提高了 18.6%和 18.0%。IHF 加载引起的形变导致高位错密度，在时效过程中为 T_1 相的析出提供了更多形核质点。经 TTIHF 处理后合金中 T_1 相的平均直径和厚度均小于其他实验条件的相应值。此外，T_1 相的密度最高且分布最均匀。

关键词：铝锂合金；形变热处理；冲击液压成形；峰时效；强化机制；位错密度

(Edited by Wei-ping CHEN)